# Comparisons of a Polymer in Confinement versus Applied Force

Liang Dai[†] and Patrick S. Doyle[‡,†,*]

[†]BioSystems and Micromechanics (BioSyM) IRG, Singapore-MIT Alliance for Research and Technology (SMART) Centre, 3 Science Drive 2, Republic of Singapore 117543

[‡]Department of Chemical Engineering, Massachusetts Institute of Technology (MIT), Cambridge, Massachusetts 02139, United States

S *Supporting Information*

ABSTRACT: The similarities and differences between geometric and tensile constraints on polymers have not been fully investigated. Here we use theory (blob models) and simulations to present a comprehensive comparison between polymers in these two situations. For a polymer in good solvent, the effect of tensile force f on extension in the Pincus regime is similar to the effect of cylindrical confinement in the de Gennes regime after mapping the characteristic length k_BT/f to the cylindrical diameter D, where k_BT is the thermal energy. However, the comparison of the effects of tension and confinement on extension is lacking when k_BT/f and D are less than the thermal blob size b, referred to as extended Pincus regime and extended de Gennes regime, respectively. In the extended Pincus regime, force can still segregate the ideal-coils with the size of $\sim k_BT/f$, resulting in the scaling of extension $L_{\parallel} \sim (k_BT/f)^{-1}$. In the extended de Gennes regime, excluded volume interaction is not sufficient to segregate the ideal-coils with the size of D, resulting in the scaling $L_{\parallel} \sim D^{-2/3}$ different from the scaling in the extended Pincus regime. In addition to the scaling of extension, the scaling of fluctuation in extension σ is also compared in the extended Pincus or extended de Gennes regime. It is found that σ is independent of f and D, which reflects the ideal-chain behavior. All of the above scaling relations are validated by Monte Carlo simulations. Simulation and scaling results are also used to determine the experimental conditions needed to access the extended de Gennes and de Gennes regimes in various single molecule experiments.
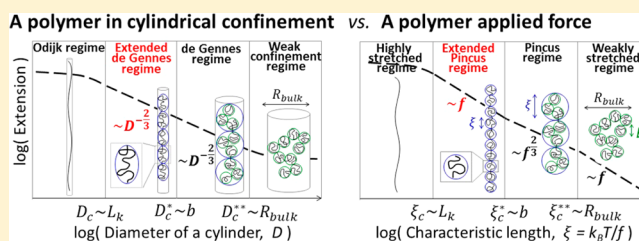
1. INTRODUCTION

Advances in single-molecule techniques have made it possible to study single polymers in geometric confinement[1−5] and under stretching force using optical/magnetic tweezers.[6−8] The responses of polymers to confinement or force provide insight into their material properties and conformation, such as the contour length,[7] the persistence length,[9,10] the interaction strength between monomers,[11,12] and the topological states.[13−16] Experimental results of polymers in confinement or under force have been used to examine polymer scaling theories[17−22] and also have many practical applications. DNA in micro-/nanofluidic devices have been applied to genome mapping, which greatly facilitates the assembling process after sequencing short fragments of DNA,[23−27] and have been applied to microfluidic separations.[28,29] DNA tweezing provides insights into the possible structural and conformational changes of DNA induced by force generated in biological processes.[6,30] Although confinement and force are different external perturbations, their effects on polymer behavior share great similarities from the viewpoint of scaling analysis[31,32] when the confinement is biaxial, such as the confinement in a cylinder or tube.

In scaling analysis, cylindrical confinement induces a characteristic length, the cylinder diameter D, to describe polymer conformation. The competition of this characteristic length D with other characteristic length scales, such as

unperturbed polymer size R_{bulk} and the Kuhn length L_k (twice the persistence length), determines the polymer behaviors in different regimes. In the de Gennes regime,[31] a polymer can be considered as a string of blobs with blob size D, as illustrated in Figure 1a. These blobs are segregated by excluded volume interactions. Within a blob, effects of confinement are absent, and thus the subchains inside a blob behave as in free solution. Combining the interblob and intrablob properties yields the scaling of polymer extension $L_{\parallel} \sim D^{-2/3}$ in the de Gennes regime.

Similar to cylindrical confinement, force applied to the end of a polymer introduces a characteristic length $\xi = k_BT/f$ to describe polymer conformations, where k_BT is the thermal energy and f is the stretching force. Under tension, a polymer can be considered as a string of tensile blobs in the Pincus regime,[32] as illustrated in Figure 1b. In contrast to cylindrical confinement, the driving force to segregate the blobs is not the excluded volume interaction between blobs but the external force. This stretching force aligns the tensile blobs because back-folding on the length scale of ξ has an associated energy cost $\sim k_BT$ and is unlikely to occur. Inside a tensile blob, the influence of external force is overwhelmed by thermal

(a) Cylindrical confinement
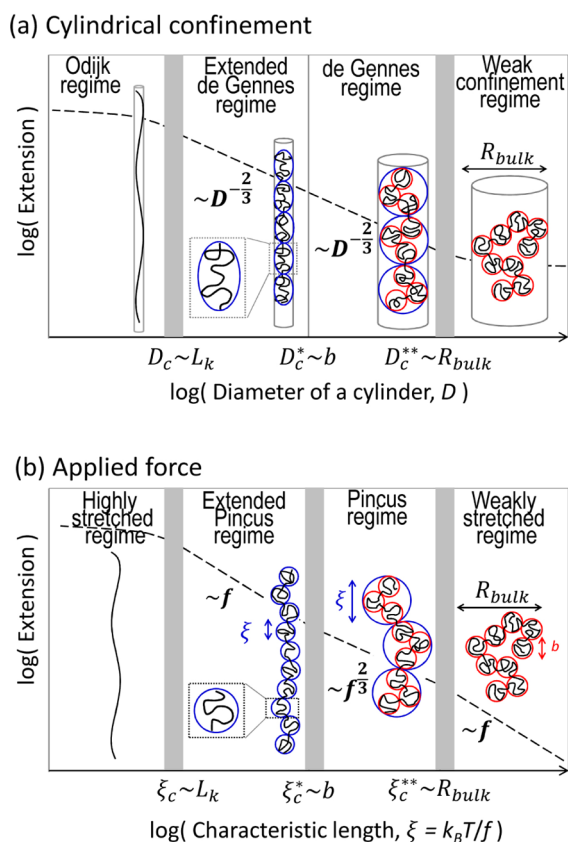

(b) Applied force

Figure 1. Schematic illustration of various regimes for a polymer in cylindrical confinement or under stretching force, where the latter is an adaptation of the illustration by McIntosh et al.[33] (a) Confinement–extension curve in log–log plot. (b) Force–extension curve in log–log plot. We use the characteristic length $\xi = k_B T/f$ instead of f for the comparison with confinement-extension curve. The gray areas indicate the transition between regimes. The red cycles denote the thermal blobs, while the blue cycles or ellipses denote the de Gennes blobs or Pincus blobs. The two zoomed-in boxes in the extended de Gennes regime and the extended Pincus regimes indicate the anisometric blob and isometric blob, respectively. The four regimes are separated by three characteristic lengths, D_c, D_c^*, D_c^{**} or ξ_c, ξ_c^*, ξ_c^{**} corresponding to the Kuhn length L_k, the thermal blob size b, and the unperturbed size R_{bulk}.

fluctuations, and thus the subchains inside a tensile blob behave as in the absence of force. Similarly, the extension scales as $L_{\parallel} \sim \xi^{-2/3} \sim f^{2/3}$ in the Pincus regime.

To arrive at the scaling $L_{\parallel} \sim D^{2/3}$ and $L_{\parallel} \sim f^{2/3}$ in the de Gennes regime and the Pincus regime, Flory scaling[34] is assumed inside blobs, i.e. the blob size D or ξ scales as $L_{blob}^{3/5}$, where L_{blob} is the contour length inside a blob. Flory scaling for polymer in good solvent is valid only when the blob size is larger than the thermal blob size b. Here, b is the critical coil size where the excluded volume interaction equals $k_B T$. The subchain with a size smaller than b behaves as an ideal chain rather than a real chain. As a result, Odijk pointed out that the size of thermal blob b is also a characteristic length which separates the polymer behavior between $D < b$ and $D > b$ or between $\xi < b$ and $\xi > b$.[35]

The unperturbed size R_{bulk}, thermal blob size b, and the Kuhn length L_k correspond to three critical lengths that separate four regimes when varying the cylindrical diameter or the stretching force, as shown in Figure 1. For a polymer under applied force, the scaling of extension in the four regimes has been described

by Netz[36] and later summarized by McIntosh and co-workers.[33] In the regime of $L_k \ll \xi \ll b$, the scaling $L_{\parallel} \sim \xi^{-1} \sim f^1$ is derived considering ideal-chain behavior inside blobs and has been recently validated by the recent experiment of stretching poly(ethylene glycol).[37] The regime of $L_k \ll \xi \ll b$ is called the ideal-coil regime by Dittmore et al.[37] and is referred to as the extended Pincus regime in the current study because we will show it is analogous to the extended de Gennes regime for a polymer in confinement.

For a polymer in confinement, the scaling behaviors in regimes $L_k \ll D \ll b$ and $b \ll D \ll R_{bulk}$ have been studied using the blob model.[35,38] In the regime $b \ll D \ll R_{bulk}$, the blob size equals D. However, in the regime $L_k \ll D \ll b$, if the blob size is still assumed to equal D (as in the de Gennes regime), blobs would interpenetrate because the excluded volume interaction energy due to the overlapping of two blobs is less than the thermal energy. This interpenetration violates the assumption of nonoverlapping blobs. To continue using the blob model in the regime $L_k \ll D \ll b$, Odijk introduced the concept of an anisometric blob,[35] which is defined with a diameter of D and a length larger than D. Later, Wang et al.[38] derived the scaling relations of free energy and extensions in the regime $L_k \ll D \ll b$. Coincidently, the scaling of extension $L_{\parallel} \sim D^{-2/3}$ the regime $L_k \ll D \ll b$ is identical to that in the regime $b \ll D \ll R_{bulk}$. The regime $L_k \ll D \ll b$ was termed the "extended de Gennes regime" by Wang et al.[38]

It is striking that the scaling of extension changes from $L_{\parallel} \sim f^{2/3}$ in the Pincus regime to $L_{\parallel} \sim f^1$ in the extended Pincus regime, while the scaling of extension remains as $L_{\parallel} \sim D^{-2/3}$ in the de Gennes and extended de Gennes regimes. Consequently, observing the scaling $L_{\parallel} \sim f^1$ in the experiments[37] and simulations[39] demonstrates the existence of the extended Pincus regime, while observing the scaling $L_{\parallel} \sim D^{-2/3}$ cannot distinguish the extended de Gennes regime from the de Gennes regime[38] and cannot prove the existence of the extended de Gennes regime. As a result, the existence of the extended de Gennes regime has yet to be confirmed.[1] Fortunately, scaling analysis predicts that the fluctuation in extension changes from $\sigma \sim D^{1/6}$ in the de Gennes regime to $\sigma \sim D^0$ in the extended de Gennes regime.[38] So the change in the scaling of fluctuation can be used to prove the existence of the extended de Gennes regime. To the best of our knowledge, there is no experiment or simulation to analyze the scaling of fluctuation from the regime $L_k \ll D \ll b$ to the regime $b \ll D \ll R_{bulk}$.

In the current study, we simulate polymers in cylindrical confinement and analyze the scaling of fluctuation to confirm the existence of the extended de Gennes regime. In addition, we also present comprehensive comparisons between polymers under force and in confinement, because the similarity between the extended Pincus regime and the extended de Gennes regime has not yet been presented. Our comparison is limited to the middle two regimes in Figure 1, because the simulation model in the current study is coarse-grained on the length of L_k and is not suitable to study the strong confinement or highly stretched regime.

2. THEORY AND COMPUTER SIMULATION

2.1. de Gennes Regime and Pincus Regime. The blob model is traditionally applied to study the scaling behaviors of polymers in confinement or under stretching force, when the confinement strength or the stretching force is within the de Gennes or the Pincus regime. Here, we summarize the scaling arguments using the blob model. We consider a polymer

Table 1. Summary of Scaling Relations of the Extension $L_{\parallel}$ and the Fluctuation σ for a Polymer in Cylindrical Confinement and under Stretching Force[a]

	cylindrical diameter	extension	fluctuation
de Gennes regime	$L_k \ll D \ll \dfrac{L_k{}^2}{w}$	$\dfrac{\langle L_{\parallel}\rangle L_k}{Lw} \approx \left(\dfrac{Dw}{L_k{}^2}\right)^{1-1/\nu}$	$\dfrac{\sigma^2}{LL_k} \approx \left(\dfrac{Dw}{L_k{}^2}\right)^{2-1/\nu}$
extended de Gennes regime	$\dfrac{L_k{}^2}{w} \ll D \ll R_{bulk}$	$\dfrac{\langle L_{\parallel}\rangle L_k}{Lw} \approx \left(\dfrac{Dw}{L_k{}^2}\right)^{1-1/\nu}$	$\sigma^2 \approx LL_k$

	applied force	extension	fluctuation
Pincus regime	$L_k \ll \dfrac{k_B T}{f} \ll \dfrac{L_k{}^2}{w}$	$\dfrac{\langle L_{\parallel}\rangle L_k}{Lw} \approx \left(\dfrac{k_B T}{f}\dfrac{w}{L_k{}^2}\right)^{1-1/\nu}$	$\dfrac{\sigma^2}{LL_k} \approx \left(\dfrac{k_B T}{f}\dfrac{w}{L_k{}^2}\right)^{2-1/\nu}$
extended Pincus regime	$\dfrac{L_k{}^2}{w} \ll \dfrac{k_B T}{f} \ll R_{bulk}$	$\dfrac{\langle L_{\parallel}\rangle}{L} \approx \dfrac{1}{3}\dfrac{fL_k}{k_B T}$	$\sigma^2 \approx LL_k$

[a]The Flory exponent is classically quoted to be $\nu = 3/5$, but has a more precise value $\nu = 0.5877 \pm 0.0006$.[43]

consisting of N_k Kuhn segments. Each Kuhn segment has a length of L_k and an effective chain width of w. The contour length is $L = N_k L_k$. The average extension is calculated as $\langle L_{\parallel}\rangle = N_{blob} R_{blob}$, where R_{blob} is the size of the blob, $N_{blob} = L/L_{blob}$ is the number of blobs, and L_{blob} is the contour length inside a blob. Using the Flory scaling $R_{blob} \approx L_{blob}{}^{3/5} L_k{}^{1/5} w^{1/5}$ inside a blob, we obtain. $\langle L_{\parallel}\rangle/L = L_k{}^{1/3} w^{1/3} R_{blob}{}^{-2/3}$ Considering that the blob size is determined by D or $k_B T/f$, we arrive at the scaling

$$\langle L_{\parallel}\rangle/L \approx D^{-2/3} L_k{}^{1/3} w^{1/3} \tag{1}$$

or

$$\langle L_{\parallel}\rangle/L \approx (k_B T/f)^{-2/3} L_k{}^{1/3} w^{1/3} \tag{2}$$

The blob model can be also applied to derive the scaling of fluctuation in extension σ. The fluctuation in size of each blob is independent, and so the total fluctuation is determined by $\sigma^2 = N_{blob}\sigma_{blob}{}^2$, where σ_{blob} is the fluctuation of a blob. Inside a blob, the influence of confinement or applied force is negligible, and we can use the formula of fluctuation for the unperturbed polymer[40] $\sigma_{blob} \approx R_{blob}$. So the scaling of the fluctuation follows $\sigma^2 = N_{blob} R_{blob}{}^2$ and is written as

$$\sigma^2 \approx L D^{1/3} L_k{}^{1/3} w^{1/3} \tag{3}$$

or

$$\sigma^2 \approx L(k_B T/f)^{1/3} L_k{}^{1/3} w^{1/3} \tag{4}$$

Alternatively, the scalings of extension and fluctuation of polymers in confinement have been derived from the renormalized free energy[38,41]

$$\frac{F}{k_B T} \approx \frac{L_{\parallel}{}^2}{L D^{1/3} L_k{}^{1/3} w^{1/3}} + \frac{L^2 L_k{}^{2/3} w^{2/3}}{L_{\parallel} D^{7/3}} \tag{5}$$

The average extension is found by minimizing the free energy. The fluctuation is related to the effective spring constant by $k_{spr}\sigma^2 \approx k_B T$, and the spring constant is determined by $k_{spr} \approx \partial^2 F/\partial L_{\parallel}{}^2$. The extension and fluctuation derived from above free energy are in agreement with eqs 1−4.

For a polymer under tension, the fluctuation can also be derived from the spring constant, which is determined by $k_{spr} = \partial f/\partial L_{\parallel}$. Then, the scaling relationship for fluctuations is solely determined by the force−extension relationship, as shown

previously by Underhill and Doyle.[42] When the force−extension scaling is $L_{\parallel} \sim f^{\alpha}$, the fluctuation scales as $\sigma^2 \sim f^{\alpha-1}$.

Note that in deriving eqs 1−4, we used the classic Flory exponent of $\nu = 3/5$. If we apply a more precise value of Flory exponent[43] of $\nu = 0.5877 \pm 0.0006$, then eqs 1 and 3 become $\langle L_{\parallel}\rangle/L \approx D^{1-1/\nu} L_k{}^{2/\nu-3} w^{2-1/\nu} = D^{-0.702} L_k{}^{0.403} w^{0.298}$ and $\sigma^2 \approx L D^{2-1/\nu} L_k{}^{2/\nu-3} w^{2-1/\nu} = D^{0.298} L_k{}^{0.403} w^{0.298}$, respectively. The exponents in eqs 2 and 4 are changed similarly.

2.2. Extended de Gennes Regime and Extended Pincus Regime. The above scaling arguments for the Pincus regime and the de Gennes regime rely on the Flory scaling inside blob. When the characteristic length D or $k_B T/f$ is less than the thermal blob size b but much larger than the Kuhn length, the subchain behaves as ideal chain on length scales smaller than D or $k_B T/f$. Such regime is referred to as the extended de Gennes regime or the extend Pincus regime because the underlying physics of the blob model remain, albeit with modifications. The size of a thermal blob is determined by setting the excluded volume (EV) interaction equal to thermal energy. Considering that the contour length inside thermal blob is $b^2 L_k{}^{-1}$ and the EV interaction in the unit of $k_B T$ is $(b^2 L_k{}^{-1})^2 w/b^3$, we attain the scaling of the thermal blob size[38]

$$b \approx L_k{}^2/w \tag{6}$$

In the case of a polymer under tension, we simply replace the scaling $R_{blob} \approx L_{blob}{}^{3/5} L_k{}^{1/5} w_k{}^{1/5}$ by $R_{blob} \approx L_{blob}{}^{1/2} L_k{}^{1/2}$. Then, the scaling for the extension becomes

$$\langle L_{\parallel}\rangle/L \approx (k_B T/f)^{-1} L_k \tag{7}$$

The fluctuation in extension can also be derived considering $R_{blob} \approx L_{blob}{}^{1/2} L_k{}^{1/2}$.

$$\sigma^2 \approx LL_k \tag{8}$$

The above equation indicates that the fluctuation in extension is independent of force and chain width in the extended Pincus regime, which reflects the ideal-chain behavior in this regime.

In the case of a polymer in confinement, we cannot simply replace the scaling of R_{blob} in the previous analysis. In the extended de Gennes regime, it costs less than thermal energy to overlap two subchains each with size D. Thus, we cannot define the subchain with a size of D as a blob. If we continue to use the blob model, we should define an anisometric blob with a diameter of D and a length larger than D so that the excluded volume interaction can segregate blobs.[35,38] The length of this

anisometric blob is determined as $R'_{blob} \approx D^{2/3}L_k{}^{2/3}w^{-1/3}$. The contour length inside the anisometric blob is $L'_{blob} \approx (R'_{blob})^2 L_k \approx D^{4/3}L_k{}^{1/3}w^{-2/3}$ due to the ideal-chain behavior inside the blob. The number of blobs becomes $N'_{blob} = L/L'_{blob}$. The extension in the extended de Gennes regime follows $\langle L_\parallel \rangle = N'_{blob}R'_{blob}$.

$$\langle L_\parallel \rangle / L \approx D^{-2/3}L_k{}^{1/3}w^{1/3} \qquad (9)$$

The above equation is identical to eq 2 in the de Gennes regime.

The fluctuation in the extended de Gennes regime is derived using $\sigma^2 \approx N'_{blob}(R'_{blob})^2$.

$$\sigma^2 \approx LL_k \qquad (10)$$

In the extended de Gennes regime, the scalings of the extension and the fluctuation have also been derived by Wang et al.[38] from the renormalized free energy. A notable feature of this analysis in the extended de Gennes regime is that the scaling of fluctuation exhibits ideal-chain behavior whereas the scaling of extension still exhibits the properties of a real-chain.

2.3. Monte Carlo Simulation. We perform Monte Carlo simulations to study a polymer under stretching force and in cylindrical confinement. To simulate as large systems as possible, we model the polymer as a chain consisting of freely jointed Kuhn segments, illustrated in Figure 2a. This model
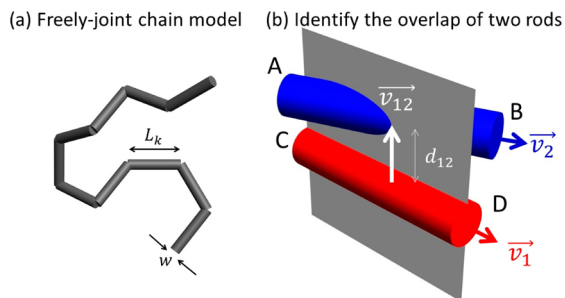

Figure 2. (a) Schematic illustration of the model for the polymer chain. (b) Schematic illustration to show how rod−rod overlapping is identified.

choice is justified as we will not be studying the Odijk regime where sub-Kuhn length behavior becomes critical. Other than the external stretching force or confining geometry, the only interaction energy in the simulation is hard-core repulsions between two segments (rods).

Rod−rod overlaps are identified when three conditions are satisfied, as illustrated by Figure 2b. First, the distance between axes of two rods must be less than the chain width. Second, we calculate the vector $\vec{v}_{12}$ that is perpendicular to the rod axis $\vec{v}_1$ and $\vec{v}_2$. We determine the plane where $\vec{v}_1$ and $\vec{v}_{12}$ are lying, as shown in Figure 2b. Both ends of the blue rod, A and B, must be located on the different sides of the plane. Third, both ends of the red rod, C and D, must be located on the different sides of the plane where $\vec{v}_2$ and $\vec{v}_{12}$ are lying. For two infinitely long rods, the first condition is enough to judge the overlap. The second and third conditions are necessary for finite length rods. This algorithm for the excluded volume interaction between rods is fast, but is so at the expense of missing some rare overlap situations (see Supporting Information).

In the case of a polymer under tension, we add an energetic term $E_{force} = -\vec{f} \cdot \vec{L}_{n2n}$, where $\vec{L}_{n2n}$ is the end-to-end vector. In the

case of a polymer in cylindrical confinement, we reject all Monte Carlo moves that place any segment outside the confining geometry.

In the simulations, the number of Kuhn segments is kept constant at 1600. Setting the Kuhn length as the unit length and $k_B T/L_k$ as the unit force, we vary the chain width and the stretching force or the cylindrical diameter. Our simulations start from a random configuration. In each Monte Carlo cycle, we perform either a crankshaft move or a reptation move, following our previous work.[44] After 10^8 equilibrium steps, we perform at least 10^9 steps in a production run. We run 30 simulations in parallel on 30 processors using different random number generator seeds. We record one polymer configuration for every 10^5 steps in each production run. For every configuration, we calculate the extension. We note that we calculate extension in slightly a different manner for confinement and stretching. For confinement, the extension is taken to be the maximum span in the direction of cylinder axis, which is widely used in the previous studies[38,45] and corresponds to the experimental measurement of polymer extension in fluidic channels using fluorescence microscopy.[46] For applied force, the extension is taken to be the end-to-end vector projected in the direction of the applied force, which corresponds to extension measured in stretching experiments using optical or magnetic tweezers. The fluctuation is calculated as the standard deviation of the extension. The self-correlation time of extension is on the order of 10^7 steps for the simulation in cylindrical confinement and on the order of 10^6 steps for the simulation under tension, and thus we sample at least 10^3-fold of correlation times for each simulation condition. The estimated statistical error of extension is always much less than the symbol size in all figures. The estimated statistical error of fluctuation is comparable to or less than the symbol size in all figures.

We employ the freely jointed chain model rather than the touching bead model used in our previous studies[13,44,45] because exploring the extended de Gennes regime or the extended Pincus regime requires a large contour length L and a small chain width w relative to the Kuhn length L_k. The number of beads in the touching bead model is determined by L/w. If we were to employ the touching bead model, the required number of beads is on the order of 10^5, exceeding our computational capabilities.

3. RESULTS AND DISCUSSIONS

3.1. Polymers in Cylindrical Confinement. First, we analyze the extension and the fluctuation as a function of the cylinder diameter using different chain widths, as shown in Figure 3, parts a and b. We recall that the contour length is $1600L_k$ in every simulation. We normalize the cylindrical diameter by the thermal blob size $L_k{}^2/w$ so that the de Gennes regime and the extended de Gennes regime are separated at the same position $Dw/L_k{}^2 \approx 1$ for all chain widths. The extension and the fluctuation are normalized such that the curves for different chain widths merge to a master curve in the de Gennes regime $Dw/L_k{}^2 \approx 1$ and the extended de Gennes regime $Dw/L_k{}^2 \ll 1$.

For all chain widths, we perform the simulations for the cylindrical diameter within $[4L_k,\ 0.7\ R_{bulk}]$ so that the extension-confinement curves follow a single-power law. Here, R_{bulk} is the radius of gyration in bulk. The condition $D > 4L_k$ is to avoid the Odijk regime and also to eliminate the error caused by the coarse-grained modeling of a smoothly
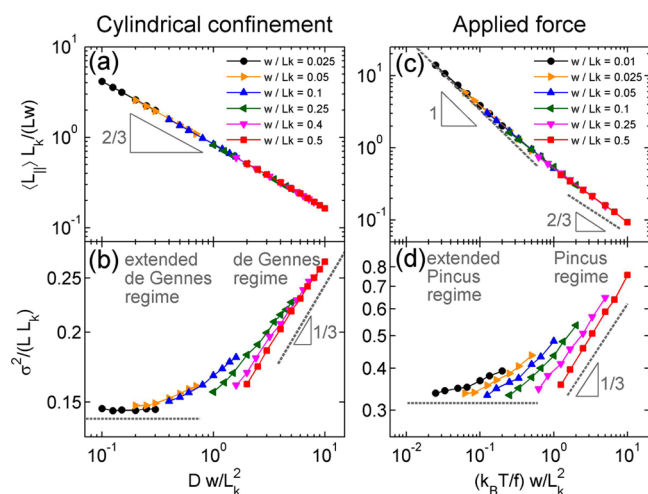
Figure 3. Normalized extension (a) and normalized square fluctuation (b) as a function of normalized cylindrical diameter in the simulations of polymers in cylindrical confinement using different chain widths. (c and d) Simulations of polymers under stretching force.

bending chain. The condition $D < 0.7R_{bulk}$ roughly corresponds to the situation of $\langle L_\parallel \rangle / D > 6$.

Figure 3a shows that the normalized extensions for different chain widths collapse to a master curve from $Dw/L_k^2 \approx 10^{-1}$ to 10, covering the transition from the extended de Gennes regime to the de Gennes regime. This master curve follows a single power law with an exponent close to $-2/3$ predicted by blob theory. The best power law fits to the data points yield the exponent of -0.672 ± 0.002, -0.679 ± 0.004, -0.687 ± 0.004, -0.698 ± 0.007, -0.702 ± 0.008, and -0.704 ± 0.009 for the dimensionless chain widths of 0.025, 0.05, 0.1, 0.25, 0.4 and 0.5, respectively. The absolute values of these exponents are slightly greater than 2/3. Recall that the scaling $L_\parallel \sim D^{-2/3}$ makes use of the Flory scaling of 3/5. If we use the precise scaling[43] of 0.5877, the scaling becomes $L_\parallel \sim D^{-0.7015}$. As expected, analysis of the extension-confinement curves does not allow one to distinguish the extended de Gennes regime from the de Gennes regime.

Next, we turn to the fluctuation in extension. The data in Figure 3b are obtained from the same simulations as Figure 3a. Different from the single-power law for the extension, the slope of the curve for the fluctuation gradually changes with D. When $Dw/L_k^2 \ll 1$, i.e., the extended de Gennes regime, the fluctuation is independent of D. When $Dw/L_k^2 \gg 1$, i.e., the de Gennes regime, the scaling agrees with the prediction $\sigma^2 \sim D^{1/3}$. The best power law fit to the simulations of $w/L_k = 0.5$ (red squares) yields the exponent of 0.31 ± 0.01. The transition from the extended de Gennes regime to de Gennes regime is gradual and broad. The curves for different chain widths collapse to a master for $Dw/L_k^2 \ll 1$ and $Dw/L_k^2 \gg 1$, but the curves diverge at the transition regime.

Combining parts a and b of Figure 3 reveals that the fluctuation is enhanced with the decreasing extension in cylindrical confinement. In contrast, the fluctuation is proportional to the extension in free solution.[40] The decreasing function for the fluctuation-extension relationship in confinement is due to the competition of N_{blob} and R_{blob}. With the increasing D, the number of blobs becomes less and each blob becomes larger. The change in N_{blob} dominates the extension $L_{blob} = N_{blob}R_{blob}$, while the change in the blob size dominates the fluctuation $\sigma^2 \approx N_{blob}R_{blob}^2$.

For an infinitely long polymer, the window size for the extended de Gennes regime depends on the relative chain width w/L_k because the extended de Gennes regime corresponds to D within $[D_c, D_c^*]$ and the window size in the log−log plot is $\log(D_c^*/D_c) \sim (L_k/w)$. For a thick chain with w close to L_k, the window size of extended de Gennes regime is vanishing small, as shown by the red-square symbols in Figure 3, part a and b. On the other hand, as $w/L_k \to 0$, i.e., approaching the ideal chain, the extended de Gennes regime becomes infinitely wide, and the de Gennes regime becomes unreachable, as shown by the black-circle symbols in Figure 3, parts a and b. Thus, tuning the value of w/L_k can change the window sizes of the extended de Gennes regime and the de Gennes regime.

3.2. Polymers under Applied Force. Parts c and d of Figure 3 show the extensions and the fluctuations for the stretching simulations using the same normalizations as parts a and b of Figure 3 with D replaced by k_BT/f. The dashed lines indicate the predicted scalings for the extended Pincus regime and the Pincus regimes regime. The strengths of stretching force in the simulations are within $[k_BT/R_{bulk}, 0.4k_BT/L_k]$. When $f < k_BT/R_{bulk}$, the polymer starts to enter the weakly stretched regime, which is indicated by the observation that $L_\parallel$ and σ^2 is no longer proportional to the contour length for a fixed force. When $f > 0.4k_BT/L_k$, the polymer starts to enter the highly stretched regime.

The normalized force−extension curves for different chain widths collapse to a master curve from $(k_BT/f)w/L_k^2 \approx 10^{-2}$ to 10^1. The slope of this master curve gradually increases with the increasing force. The best power law fit to the data of the thickest chain (red squares in Figure 3c) yields an exponent of -0.72 ± 0.02, which is in agreement of theoretical prediction of $-2/3$. For comparison, the exponent obtained from the experiment of stretching poly(ethylene glycol) is -0.69 ± 0.08.[37] The best power law fit to the data of thinnest chain (black circles) yields an exponent of -0.93 ± 0.01. The dashed line with the slope of -1 in Figure 3c corresponds to the exact solution $3\langle L_\parallel \rangle/L = fL_k/k_BT$ for the ideal chain under small force. The normalized force−extension curves approach this dashed line with the decreasing abscissa and merge with the dashed line at $(k_BT/f)w/L_k^2 \approx 0.01$. The transition from the Pincus regime to the extended Pincus regime is gradual.

The normalized fluctuation also gradually changes with $(k_BT/f)w/L_k^2$. The trends are in agreement with the theoretical predictions. In the extended Pincus regime with $(k_BT/f)w/L_k^2 \ll 1$, the fluctuation is independent of f. The fluctuation data approach the horizontal dashed line with the decreasing $(k_BT/f)w/L_k^2$. In the Pincus regime, the best power law fit to the thickest chain (red squares) yields the exponent of 0.36 ± 0.01, close to the theoretical prediction of 1/3. The curves for different chain widths in Figure 3d do not fully collapse; however, it is expected that they will more completely overlap if we extend the curves to smaller or larger abscissa values because the scaling analysis predicts $\sigma^2 \approx L (k_BT/f)^{1/3}L_k^{1/3}w^{1/3}$ for the Pincus regime and $\sigma^2 \approx LL_k$ for the extended Pincus regime.

In Figure 4, we plot the force−extension curves using a different normalization of force. The forces in Figure 4 are over a wider range than the forces in Figure 3, parts c and d, in order to show the behavior beyond the Pincus and the extended Pincus regimes. In addition, parts a and b of Figure 4 include the curve for the simulation of an ideal chain with $w = 0$ (turning off the excluded volume interaction). When $f <$
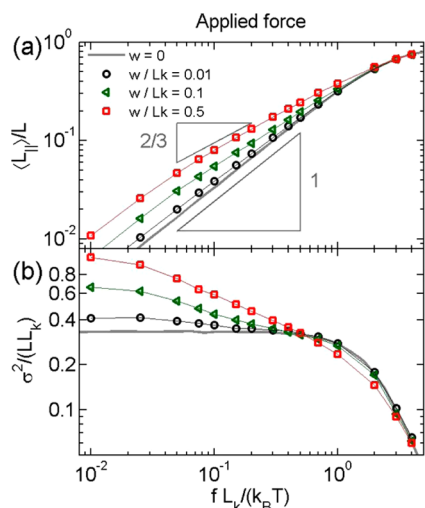
Figure 4. (a) Normalized extension as a function of normalized force in the simulations of polymers under stretching force using different chain widths. (b) Normalized square fluctuation as a function of normalized force for the same simulations.

$0.4k_BT/L_k$, the force−extension curve for the ideal chain is very well approximated by $3\langle L_\parallel \rangle/L = fL_k/k_BT$, where the extension is proportional to the force. As expected, all force−extension curves merge to the curve of the ideal chain when the stretching force is larger than a critical value f_c^*. This critical value depends on the chain width. For the thin chain, the critical force is less than $0.4k_BT/L_k$. In this case, $f \in [0.4k_BT/L_k, f_c^*]$ is the extended Pincus regime. For a thick chain, f_c^* is larger than $0.4k_BT/L_k$, and then the extended Pincus regime will be skipped when varying the force.

Figure 5 compares the force−extension curves obtained from our simulations and the experiment by Dittmore et al.[37] Forces
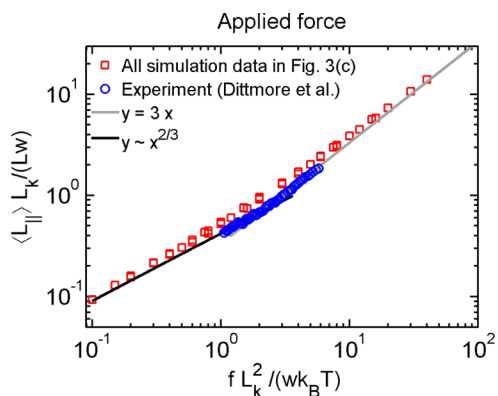

Figure 5. Comparison of normalized force−extension curves from simulations and experiments. The simulation points comprise all the data in Figure 3c. The experimental data points are replotted from the force−extension data by Dittmore et al.[37] using $L = 570$ nm; $L_k = 1.1$ nm, and $w = 0.1$ nm in normalizations. The gray line and the black line were used to by Dittmore et al. to fit the data in two regimes.

and extensions are normalized such that the force−extension curve is independent of w/L_k in the Pincus regime and the extended Pincus regime. The simulation data points are copied from Figure 3c. Poly(ethylene glycol) was used in the stretching experiment. Dittmore et al. fitted the force−extension data in the extended Pincus regime to $3\langle L_\parallel \rangle/L = fL_k/k_BT$ and determined the Kuhn length of 1.1 nm. Dittmore

et al. also estimated the excluded volume interaction parameter as 0.2 nm³ from the crossover force between the Pincus regime and the extended Pincus regime. The excluded volume interaction parameter is related to the chain width as $\pi L_k^2 w/2$,[47] and so we estimate the effective chain width is about 0.1 nm. Using this effective chain width, we replot the experimental data from Dittmore et al. in Figure 5. The two gray lines are the fit lines used by Dittmore et al. The asymptotic behavior of our simulation data matches the two fit lines. However, the transition from the Pincus regime to the extended Pincus regime is much broader in our simulations than in experiments. One possible reason is that we use a simple hard-core repulsion for the segment−segment interaction. The gradual transition has also been observed in the recent simulations using a lattice model.[39] We calculated the effective chain width in the experiment of Dittmore et al. from the excluded volume interaction parameter, which itself was obtained from a scaling estimate containing an unknown, presumed to be of order unity, numerical prefactor. If an effective chain width different from 0.1 nm is used in Figure 5, the gray line will be unaffected, and the black line will be shifted up or down with a fixed slope.

The above analysis only considered polymer properties in the longitudinal direction. Significant differences are expected in the transverse direction. Because of the lateral freedom of the blobs (Figure 1), a polymer under applied force will have larger fluctuations in the transverse directions compared to a polymer in confinement. This is confirmed in our simulation results (Supporting Information). We remind the reader that the ends of the chain are not held fixed in the constant force simulations

3.3. Implications for Single Molecule Experiments. Many stretching and confinement experiments use double-stranded DNA (ds-DNA) as a model polymer.[7,18,46,48] Our simulation results and scaling analysis can be used to understand which regimes ds-DNA is located in for given experimental conditions, and conversely, to estimate parameters for exploring a certain regime in future experiments. The Kuhn length of bare DNA is about 100 nm[9] and does not appreciably change upon staining with a fluorescent dye.[49] The effective chain width depends on the ionic strength. For a typical ionic strength of 50 mM, the effective chain width is about 7 nm.[12,50] The following estimations are based on $L_k = 100$ nm and $w = 7$ nm except otherwise specified.

First, we consider the experiments of ds-DNA in fluidic channels. The minimum channel width to explore the de Gennes regime is approximately $D_c^* \approx b \approx L_k^2/w = 1429$ nm. The determination of D_c^* is arbitrary to within an order 1 constant due to the broad transition between the de Gennes and the extended de Gennes regimes (Figure 3b). Our selection of $D_c^* \approx L_k^2/w$ is located at the middle of the transition. The exact value of the minimum channel width D_c for the extended de Gennes regime cannot be obtained from the simulation results in the current study because we use a coarse-grained model and only explore $D \geq 4L_k$. We can know the upper bound of D_c is $4L_k$ because the scaling $L_\parallel \sim D^{-2/3}$ is valid for $D \geq 4L_k$. The lower bound of D_c is $2L_k$ based on the observation in our previous simulations[45] of 8 μm DNA using the touching bead model because the scaling $L_\parallel \sim D^{-2/3}$ was not reached at $D = 2L_k$. The relevant data is shown in the Supporting Information. Combining the upper and the lower bounds, the uncertainty of D_c is within a factor of 2. We use the upper bound $D_c = 4L_k$ in the following estimation, because the de Gennes scaling $L_\parallel \sim D^{-2/3}$ has never been observed in experiments and we hope our estimation can help find the

experimental conditions to observe the scaling. If we use the lower bound for D_c, then we are not certain that the de Gennes scaling can be observed for $D > D_c$.

After obtaining D_c^* and D_c, we estimate the minimum contour lengths to enter the de Gennes and the extended de Gennes regimes, D_c^{**}, and L_c^*. We assume $L_\parallel/D \geq 6$ must be satisfied for the blob model to be applicable, just as in the simulations. The value of $L_\parallel$ can be obtained from the master curve in Figure 3a, which is accurately described by $\langle L_\parallel \rangle L_k/Lw = 0.83(Dw/L_k^2)^{-0.7015}$. This equation is obtained by fitting the prefactor while the exponent is fixed as $1/\nu - 1 = 0.7015$ with the precise Flory scaling $\nu = 0.5877$. This master equation can be used to infer the effective chain width after measuring the extension in a certain channel size. Inputting the parameters $w = 7$ nm, $L_k = 100$ nm, and the condition $L_\parallel = 6D$ into the equation $\langle L_\parallel \rangle L_k/Lw = 0.83(Dw/L_k^2)^{-0.7015}$, we obtain $L_c^* \approx 17$ μm when $D = 400$ nm, and the parameter $L_c^{**} \approx 148$ when $D = 1429$ nm. Note that if we use lower bound of $D_c = 200$ nm, L_c^* becomes approximately 5.2 μm. This means ds-DNA should be at least approximately 17 μm to enter the extended de Gennes regime and at least approximately 148 μm to enter the de Gennes regime for the typical ionic strength around 50 mM. As an aside, we note that Latinwo and Schroeder[51] recently estimated the contour length inside a thermal blob to be approximately 575 μm by considering the Kuhn length as 132 nm and taking the width as the bare ds-DNA diameter of 2 nm. Their quoted width does not correspond to most experimental conditions and the Kuhn length of DNA has shown to be unaffected (remaining at a value of about 104 nm) by intercalation of fluorescent dyes (e.g., YOYO-1).[49]

Many experiments used λ-DNA with a fluorophore stained contour length of 21 μm. As the channel width decreases, λ-DNA will jump from the weak confinement regime to the extended de Gennes regime, skipping the de Gennes regime altogether. Furthermore, the window size for the extended de Gennes regime is quite narrow because the contour length 21 μm is only slightly larger than $L_c \approx 17$ μm. As a result, the scaling $L_\parallel \sim D^{-2/3}$ was not observed in the experiments of λ-DNA.[46,48] Persson et al.[48] also used T4-DNA (72 μm when stained) in experiments.[48] On the basis of the calculation in the previous paragraph, it is expected to observe the scaling $L_\parallel \sim D^{-2/3}$ for T4-DNA in the channel with the width from 400 to 900 nm (extended de Gennes regime). However, the channel size was only varied from 90 to 260 nm by Persson et al. The best-power law fits to the extension-confinement curves in experiments of λ-DNA and T4DNA yielded the exponents from 0.78 to 0.85.[46,48] A more recent experiment using slightly larger channels found an exponent of -0.77 ± 0.05, slightly closer to the de Gennes scaling.[52] This exponents are significantly larger than 2/3 because they are fit to data in the transition from strong confinement to the extended de Gennes regime.[38,45]

For T4-DNA at moderate ionic strength around 50 mM, the extended de Gennes regime exists from $D = 400-900$ nm, but the de Gennes regime is skipped when varying D. Exploring the de Gennes regime using T4-DNA is feasible under very low ionic strength. For instance, when the ionic strength is 1 mM, the effective chain width is approximately 54 nm,[12,50] and the Kuhn length is approximately 158 nm using the Odijk−Skolnick−Fixman equation.[53,54] Then, the two critical channel sizes are $D_c = 4L_k = 632$ nm and $D_c^* = L_k^2/w = 462$ nm . Since $D_c > D_c^*$, T4-DNA will skip the extended de Gennes regime and jump from the strong confinement to the de Gennes regime at

$D = 632$ nm when increasing the channel size. The upper bound of D for the de Gennes regime corresponds to the channel size satisfying $L_\parallel = 6D$, which is approximately 1500 nm using the relationship $\langle L_\parallel \rangle L_k/L_w = 0.83 (Dw/L_k^2)^{0.7015}$.

In addition to the extension, it is of great interest to measure the fluctuation in extension as a function of the channel width. Su et al.[55] measured the fluctuations in extension for λ-DNA and T4-DNA in nanochannels, but in their studies they did not greatly vary the channel dimension. Thus, it is difficult to examine the D-dependence of fluctuation from their data. For T4-DNA, it is predicted by our simulations and scaling analysis that the fluctuation is almost independent of the channel size from 400 to 900 nm when the ionic strength is 50 mM, and that the fluctuation scales as $\sigma^2 \sim D^{1/3}$ from 632 to 1500 nm when the ionic strength is 1 mM.

Next, we consider the stretching experiment using double-stranded DNA. Two characteristic forces are $f_c \sim k_BT/L_K \approx 0.04$ pN and $f_c^* \sim k_BT/b \approx 0.02$ pN. These values are close to or less than the minimum force applied in magnetic or optical tweezers. So it is not suitable to use double-stranded DNA to study the Pincus and the extended Pincus regimes, as mentioned previously by Marko and Siggia.[10] The polymer used by Dittmore and co-workers[37] to study the transition from the Pincus regime to the extended Pincus regime is poly(ethylene glycol) with a Kuhn length of approximately 1 nm. Single-stranded DNA (ss-DNA) has a Kuhn length of 1.24 nm under the ionic strength of 3 M, where the electrostatic contribution to the Kuhn length is vanishingly small.[56] Thus, ss-DNA[57] is also a candidate polymer to explore the Pincus regime and the extended Pincus regime. Note that the fluctuations referred in the current study are always in the longitudinal (applied force) direction. The transverse fluctuations provide additional information.[42,58]

In addition to the scalings of static properties, the scalings of dynamics are also expected to be different for the de Gennes/Pincus regime and the extended de Gennes/Pincus regime. The relaxation time is determined by $\tau \approx \zeta/k_{spr}$, where ζ is the polymer drag coefficient and k_{spr} is the effective spring constant.[38] As mentioned in section 2.1, k_{spr} and σ are related by $k_{spr}\sigma^2 \approx k_BT$, so the change in the scaling of fluctuation is directly related to the change in the scaling of k_{spr}, which affects the scaling of τ. Using simulations, Radhakrishman and Underhill investigated the different relaxation times in the Pincus and the extended Pincus regimes.[59] It is also expected that the relaxation dynamics change from the de Gennes regime to the extended de Gennes regime for a polymer in confinement. If we assume the polymer drag coefficient is proportional to the extension $\zeta \sim L_\parallel \approx D^{-2/3}LL_k^{1/3}w^{1/3}$, then we can predict the scaling of relaxation time changes from $\tau \sim D^{-1/3} L^2L_k^{2/3}w^{2/3}$ in the de Gennes regime to $\tau \sim D^{-2/3} L^2L_k^{4/3}w^{1/3}$ in the extended de Gennes regime.[38]

4. CONCLUSIONS

Polymers pulled by their ends and confined to tubes have some subtle differences that were shown by comparing the scaling relations of both extension and fluctuations. Importantly, fluctuations allow us to prove the existence of the newly postulated extended de Gennes regime.[35,38] The extended de Gennes regime is analogous to the extended Pincus regime for a polymer under force. However, the scaling of extension in the extended Gennes regime is different from that in the extended Pincus regime because the polymer stretching in these two situations are driven by the excluded volume interaction and

external force, respectively. Our comparison between confinement and tension is limited to the classic/extended de Gennes/Pincus regimes due to the coarse-graining model used in our simulations. It will be of future interest to compare the confinement and tension in the transition regime where the characteristic lengths D and $k_B T/f$ are close to the Kuhn length L_k, because this regime is more relevant to the experiments of double-stranded DNA in confinement and nanofluidic devices used for genome mapping.

Our analysis suggests that λ-DNA, which is often used in the confinement experiments, is too short to enter the de Gennes regime. Even for the extended de Gennes regime, the corresponding range of channel size is rather small. It is feasible to explore the extended de Gennes regime using T4-DNA in high-salt solution, and also feasible to explore the de Gennes regime using T4-DNA in low-salt solution. Although the physics for the de Gennes regime and the extended de Gennes regime are different, the scalings of extension coincidently match each other. Distinguishing the extended de Gennes regime from the de Gennes regime can be achieved by measuring the scaling of fluctuations. Furthermore, transitioning from the de Gennes regime to the extended de Gennes regime is expected to affect the scaling of relaxation time, which is related to the fluctuation in extension.

■ ASSOCIATED CONTENT

Ⓢ Supporting Information

Algorithm used to identify the rod−rod overlapping in simulations, transverse fluctuations of polymers in simulations, and previous simulation results. This material is available free of charge via the Internet at http://pubs.acs.org.

■ AUTHOR INFORMATION

Corresponding Author
*E-mail: (P.S.D.) pdoyle@mit.edu.
Notes
The authors declare no competing financial interest.

■ ACKNOWLEDGMENTS

■ REFERENCES

(1) Reisner, W.; Pedersen, J. N.; Austin, R. H. *Rep. Prog. Phys.* **2012**, *75*, 106601.

(2) Tegenfeldt, J. O.; Prinz, C.; Cao, H.; Chou, S.; Reisner, W. W.; Riehn, R.; Wang, Y. M.; Cox, E. C.; Sturm, J. C.; Silberzan, P.; Austin, R. H. *Proc. Natl. Acad. Sci. U.S.A.* **2004**, *101*, 10979−10983.

(3) Reisner, W.; Larsen, N. B.; Flyvbjerg, H.; Tegenfeldt, J. O.; Kristensen, A. *Proc. Natl. Acad. Sci. U.S.A.* **2009**, *106*, 79−84.

(4) Jo, K.; Dhingra, D. M.; Odijk, T.; de Pablo, J. J.; Graham, M. D.; Runnheim, R.; Forrest, D.; Schwartz, D. C. *Proc. Natl. Acad. Sci. U.S.A.* **2007**, *104*, 2673−2678.

(5) Kim, Y.; Kim, K. S.; Kounovsky, K. L.; Chang, R.; Jung, G. Y.; dePablo, J. J.; Jo, K.; Schwartz, D. C. *Lab Chip* **2011**, *11*, 1721−1729.

(6) Smith, S. B.; Cui, Y. J.; Bustamante, C. *Science* **1996**, *271*, 795−799.

(7) Smith, S. B.; Finzi, L.; Bustamante, C. *Science* **1992**, *258*, 1122−1126.

(8) Wang, M. D.; Yin, H.; Landick, R.; Gelles, J.; Block, S. M. *Biophys. J.* **1997**, *72*, 1335−1346.

(9) Bustamante, C.; Marko, J. F.; Siggia, E. D.; Smith, S. *Science* **1994**, *265*, 1599−1600.

(10) Marko, J. F.; Siggia, E. D. *Macromolecules* **1995**, *28*, 8759−8770.

(11) Zhang, C.; Zhang, F.; van Kan, J. A.; van der Maarel, J. R. C. *J. Chem. Phys.* **2008**, *128*, 225109.

(12) Hsieh, C. C.; Balducci, A.; Doyle, P. S. *Nano Lett.* **2008**, *8*, 1683−1688.

(13) Dai, L.; van der Maarel, J. R. C.; Doyle, P. S. *ACS Macro Lett.* **2012**, *1*, 732−736.

(14) Micheletti, C.; Marenduzzo, D.; Orlandini, E. *Phys Rep* **2011**, *504*, 1−73.

(15) Lin, P. K.; Chang, J.-F.; Wei, C.-H.; Tsao, P. H.; Fann, W. S.; Chen, Y.-L. *Phys. Rev. E* **2011**, *84*, 031917.

(16) Strychalski, E. A.; Geist, J.; Gaitan, M.; Locascio, L. E.; Stavis, S. M. *Macromolecules* **2012**, *45*, 1602−1611.

(17) Dai, L.; Tree, D. R.; van der Maarel, J. R. C.; Dorfman, K. D.; Doyle, P. S. *Phys. Rev. Lett.* **2013**, *110*, 168105.

(18) Tang, J.; Levy, S. L.; Trahan, D. W.; Jones, J. J.; Craighead, H. G.; Doyle, P. S. *Macromolecules* **2010**, *43*, 7368−7377.

(19) Balducci, A.; Mao, P.; Han, J. Y.; Doyle, P. S. *Macromolecules* **2006**, *39*, 6273−6281.

(20) Bonthuis, D. J.; Meyer, C.; Stein, D.; Dekker, C. *Phys. Rev. Lett.* **2008**, *101*, 108303.

(21) Chen, Y.-L.; Graham, M. D.; de Pablo, J. J.; Randall, G. C.; Doyle, P. S. *Phys. Rev. E* **2004**, *70*, 060901.

(22) Strychalski, E. A.; Levy, S. L.; Craighead, H. G. *Macromolecules* **2008**, *41*, 7716−7721.

(23) Lam, E. T.; Hastie, A.; Lin, C.; Ehrlich, D.; Das, S. K.; Austin, M. D.; Deshpande, P.; Cao, H.; Nagarajan, N.; Xiao, M.; Kwok, P. Y. *Nat. Biotechnol.* **2012**, *30*, 771−776.

(24) Marie, R.; Pedersen, J. N.; Bauer, D. L.; Rasmussen, K. H.; Yusuf, M.; Volpi, E.; Flyvbjerg, H.; Kristensen, A.; Mir, K. U. *Proc. Natl. Acad. Sci.* **2013**, DOI: 10.1073/pnas.1214570110.

(25) Michaeli, Y.; Ebenstein, Y. *Nat. Biotechnol.* **2012**, *30*, 762−763.

(26) Ostergaard, P. F.; Matteucci, M.; Reisner, W.; Taboryski, R. *Analyst* **2013**, *138*, 1249−1255.

(27) Dorfman, K. D. *AIChE J.* **2013**, *59*, 346−354.

(28) Dorfman, K. D.; King, S. B.; Olson, D. W.; Thomas, J. D. P.; Tree, D. R. *Chem. Rev.* **2013**, *113*, 2584−2667.

(29) Dorfman, K. D. *Rev. Mod. Phys.* **2010**, *82*, 2903−2947.

(30) Zhang, X.; Chen, H.; Fu, H.; Doyle, P. S.; Yan, J. *Proc. Natl. Acad. Sci. U.S.A.* **2012**, *109*, 8103−8108.

(31) de Gennes, P. G. *Scaling concepts in polymer physics*; Cornell University Press: Ithaca, NY, 1979.

(32) Pincus, P. *Macromolecules* **1976**, *9*, 386−388.

(33) McIntosh, D. B.; Ribeck, N.; Saleh, O. A. *Phys. Rev. E* **2009**, *80*, 051401.

(34) Flory, P. J. *J. Chem. Phys.* **1942**, *10*, 51.

(35) Odijk, T. *Phys. Rev. E* **2008**, *77*, 060901.

(36) Netz, R. R. *Macromolecules* **2001**, *34*, 7522−7529.

(37) Dittmore, A.; McIntosh, D. B.; Halliday, S.; Saleh, O. A. *Phys. Rev. Lett.* **2011**, *107*, 148301.

(38) Wang, Y.; Tree, D. R.; Dorfman, K. D. *Macromolecules* **2011**, *44*, 6594−6604.

(39) Hsu, H. P.; Binder, K. *J. Chem. Phys.* **2012**, *136*, 024901.

(40) de Gennes, P. G. *Macromolecules* **1976**, *9*, 587−593.

(41) Jun, S.; Thirumalai, D.; Ha, B. Y. *Phys. Rev. Lett.* **2008**, *101*, 138101.

(42) Underhill, P. T.; Doyle, P. S. *J Non-Newton Fluid* **2004**, *122*, 3−31.

(43) Li, B.; Madras, N.; Sokal, A. D. *J. Stat. Phys.* **1995**, *80*, 661−754.

(44) Dai, L.; Jones, J. J.; van der Maarel, J. R. C.; Doyle, P. S. *Soft Matter* **2012**, *8*, 2972−2982.

(45) Dai, L.; Ng, S. Y.; Doyle, P. S.; van der Maarel, J. R. C. *ACS Macro Lett.* **2012**, *1*, 1046−1050.

(46) Reisner, W.; Morton, K. J.; Riehn, R.; Wang, Y. M.; Yu, Z.; Rosen, M.; Sturm, J. C.; Chou, S. Y.; Frey, E.; Austin, R. H. *Phys. Rev. Lett.* **2005**, *94*, 196101.

(47) Onsager, L. *Ann. N.Y. Acad. Sci.* **1949**, *51*, 627−659.

(48) Persson, F.; Utko, P.; Reisner, W.; Larsen, N. B.; Kristensen, A. *Nano Lett.* **2009**, *9*, 1382−1385.

(49) Gunther, K.; Mertig, M.; Seidel, R. *Nucleic Acids Res.* **2010**, *38*, 6526−6532.

(50) Stigter, D. *Biopolymers* **1977**, *16*, 1435−1448.

(51) Latinwo, F.; Schroeder, C. M. *Soft Matter* **2011**, *7*, 7907−7913.

(52) Utko, P.; Persson, F.; Kristensen, A.; Larsen, N. B. *Lab Chip* **2011**, *11*, 303−308.

(53) Odijk, T. *J. Polym. Sci., Polym. Phys.* **1977**, *15*, 477−483.

(54) Skolnick, J.; Fixman, M. *Macromolecules* **1977**, *10*, 944−948.

(55) Su, T. X.; Das, S. K.; Xiao, M.; Purohit, P. K. *PLOS One* **2011**, *6*, e16890.

(56) Saleh, O. A.; McIntosh, D. B.; Pincus, P.; Ribeck, N. *Phys. Rev. Lett.* **2009**, *102*, 068301.

(57) Brockman, C.; Kim, S. J.; Schroeder, C. M. *Soft Matter* **2011**, *7*, 8005−8012.

(58) Baba, T.; Sakaue, T.; Murayama, Y. *Macromolecules* **2012**, *45*, 2857−2862.

(59) Radhakrishnan, R.; Underhill, P. T. *Soft Matter* **2012**, *8*, 6991−7003.